

The Reversibility Of Magnetic Reconnection

M. Xuan,¹ M. Swisdak,^{1, a)} and J. F. Drake¹

*Institute for Research in Electronics and Applied Physics, University of Maryland,
College Park, MD 20742*

(Dated: 31 March 2021)

The reversibility of the transfer of energy from the magnetic field to the surrounding plasma during magnetic reconnection is examined. Trajectories of test particles in an analytic model of the fields demonstrate that irreversibility is associated with separatrix crossings and regions of weaker magnetic field. Inclusion of a guide field increases the degree of reversibility. Full kinetic simulations with a particle-in-cell code support these results and demonstrate that while time-reversed simulations at first “un-reconnect”, they eventually evolve into a reconnecting state.

arXiv:2103.16393v1 [physics.plasm-ph] 30 Mar 2021

^{a)}Electronic mail: swisdak@umd.edu

I. INTRODUCTION

The mean free path associated with classical collisions significantly exceeds the typical scale sizes in many heliospheric and astrophysical plasmas. This simple observation raises interesting questions as to how energy dissipates in these systems, particularly for phenomena such as magnetic reconnection¹⁻³, turbulence⁴, and shocks⁵ in which kinetic scales are important. In the complete absence of collisions, Boltzmann's equation describing the evolution of the distribution function f reduces to the Vlasov equation, which is formally reversible in time. Reversibility implies, among other things, that in a closed system the entropy – and in fact any function of f – remains constant during the system's evolution. Despite this restrictive mathematical constraint, Landau⁶ demonstrated that one-dimensional electrostatic plasma waves in the nominally collisionless limit are accompanied by a cascade to smaller and smaller structures in phase space which, in an actual plasma, inevitably lead to dissipation, irreversibility, and an increase in entropy. Landau damping has been experimentally confirmed⁷ and subsequent work has shown that the same basic mechanism occurs in association with many other plasma oscillations^{8,9}.

The example of Landau damping demonstrates that mathematically reversible processes can, in fact, lead to irreversibility in real systems. An interesting question is whether that conclusion extends to the phenomenon of magnetic reconnection. During reconnection a change in magnetic topology triggers a transfer of energy from the field to the surrounding plasma as slowly inflowing plasma crosses magnetic separatrices and is accelerated to Alfvénic velocities flowing away from an X-point¹⁰. In a strictly collisionless Vlasov-governed system the transfer of energy from field to particles is completely reversible, implying that it should be possible for reconnection to run backwards, with Alfvénic plasma jets converging at the X-point accompanied by a transfer of energy from the plasma to the magnetic field (i.e., reversed reconnection would act as a dynamo). This sequence of events is not observed in nature, suggesting that, in practice if not in theory, collisionless magnetic reconnection is irreversible.

Data from the Magnetospheric Multiscale (MMS) Mission have demonstrated close agreement between in situ observations of reconnection and the results of particle-in-cell (PIC) simulations¹¹⁻¹³. Such simulations follow macroparticles as they move through their collective self-consistent electromagnetic fields interpolated to a numerical grid and, in principle, capture all of the important dynamics in reconnecting plasmas. Since, as with the (assumed to be collisionless) physical system, the equations evolved in PIC codes are time-reversible, examining questions concern-

ing reversibility in PIC simulations serves as a useful proxy for actual reconnection. We will show below that reconnection behaves irreversibly in such simulations. In Section II we discuss test-particle trajectories in a simple analytic model of reconnection. Section III describes self-consistent particle-in-cell simulations of reconnection run forward and backward in time while Section IV discusses the results and their broader implications.

II. TEST PARTICLE TRAJECTORIES

Particle trajectories in self-consistent PIC simulations will be discussed below, but we first consider a simpler model that captures the key features of fields near a reconnection X-point. Observations and simulations have demonstrated that reconnection in a fully three-dimensional domain is often accompanied by turbulence and complicated field line trajectories^{12,14}. Despite the complexity, however, many important features of reconnection, including the large-scale topology and the reconnection rate, remain similar to what is observed in simulations with reduced domains, sometimes called 2.5D, in which variations perpendicular to the reconnection plane are suppressed¹⁵. Since, as we will show, reconnection is irreversible in such restricted domains it seems clear that it will also be irreversible in a fully three-dimensional system.

A. Model

With that motivation we seek a simple model of a reconnection X-point in a system with an invariant direction, here parallel to $\hat{\mathbf{y}}$. Two cases are of interest: Anti-parallel reconnection, in which the reconnecting fields, which lie parallel to $\hat{\mathbf{x}}$, have a shear angle of 180° ; and guide-field reconnection in which a spatially constant out-of-plane component of the magnetic field reduces the shear angle.

We consider a dimensionless model, i.e., one in which every variable is associated with a suppressed scaling factor that carries information about the proper units. Let the only non-zero component of the vector potential have the form

$$A_y = -\frac{1}{2} (z^2 - \alpha_B x^2) - \alpha_E t \quad (1)$$

where α_B and α_E are positive constants and the electrostatic potential $\phi = 0$. The magnetic and electric fields are then

$$\mathbf{B} = z\hat{\mathbf{x}} + \alpha_B x\hat{\mathbf{z}} \quad \mathbf{E} = \alpha_E \hat{\mathbf{y}} \quad (2)$$

Since E_y , which is equivalent to the reconnection rate, is constant in space, Faraday's Law and the invariance with respect to y imply \mathbf{B} is stationary in time. No guide field is present so the unreconnected fields on either side of the current layer are anti-parallel and $E_{\parallel} = (\mathbf{E} \cdot \mathbf{B})/B$ trivially vanishes everywhere. Ellipses centered at the origin mark contours of constant magnetic field strength. Magnetic separatrices along the lines $z = \pm\sqrt{\alpha_B}x$ divide space into upstream ($|z| > \sqrt{\alpha_B}|x|$) and downstream ($|z| < \sqrt{\alpha_B}|x|$) regions. Similar configurations have previously been investigated as models of reconnection^{16,17}.

Generally speaking, the two instances of α in equation 1 can take different values with α_B related to the angle of the separatrices and α_E to the reconnection rate. (If, for example, $\alpha_B = 1$ and $\alpha_E = 0$ then the field lines meet at right angles at the X-point, the associated current vanishes, and reconnection does not occur.) However,¹⁸ has argued that constraints at magnetohydrodynamic scales impose the condition $\alpha_E \approx \alpha_B$ when $\alpha_B \ll 1$. In this work we choose $\alpha_B = \alpha_E = \alpha = 0.1$.

The symmetry inherent in the reconnection of anti-parallel fields is broken by an out-of-plane (guide) component, which can in practice have significant effects even when relatively small in magnitude¹⁹. Including a constant $B_y \neq 0$ while maintaining the condition $E_{\parallel} = 0$ implies the existence of non-zero in-plane electric fields. An electrostatic potential ϕ , with $\mathbf{E} = -\nabla\phi$, generating these components satisfies

$$-z \frac{\partial \phi}{\partial x} - \alpha x \frac{\partial \phi}{\partial z} + \alpha B_y = 0 \quad (3)$$

the solution to which can be found from the method of characteristics to be

$$\phi = \sqrt{\alpha} B_y \log |z + \sqrt{\alpha}x| + g(z^2 - \alpha x^2) \quad (4)$$

with g an arbitrary function that can, in general, be chosen to satisfy boundary conditions but will be neglected here. The resulting in-plane components of \mathbf{E} are

$$E_x = -\alpha \frac{B_y}{z + \sqrt{\alpha}x} \quad E_z = -\sqrt{\alpha} \frac{B_y}{z + \sqrt{\alpha}x} \quad (5)$$

In-plane contours of the $\mathbf{E} \times \mathbf{B}$ flow and magnetic field lines for the case $B_y = 1$ are shown in Figure 1. Interestingly, despite the simplicity of the model, there are striking similarities to particle-in-cell simulations of guide-field reconnection²⁰, including strong flows across the $z = \sqrt{\alpha}x$ separatrix and weak sheared flows straddling $z = -\sqrt{\alpha}x$.

The existence of singularities in ϕ , E_x , and E_z along the $z = -\sqrt{\alpha}x$ separatrix has deeper roots than the specific choices of functional forms assumed in this model. First note that it is not possible

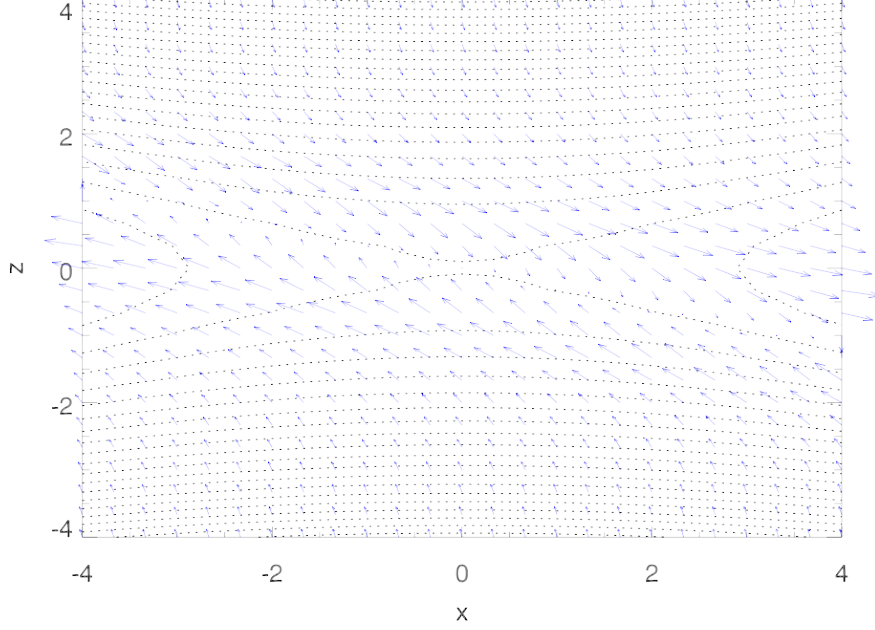


FIG. 1. Magnetic field lines (dashed) and in-plane $\mathbf{E} \times \mathbf{B}$ flow vectors (solid blue) for the analytic model with $\alpha = 0.1$ and $B_g = 1$.

to choose a g in equation 4 that eliminates the singularities. Since g is only a function of $z^2 - \alpha x^2$, it has the same magnitude on both $z = \sqrt{\alpha}x$ and $z = -\sqrt{\alpha}x$ so that any cancellation along the latter will create a new singularity on the former. More generally, any 2.5D model with a time-stationary magnetic field that includes a spatially constant out-of-plane component and satisfies $\mathbf{E} \cdot \mathbf{B} = 0$ must have singularities associated with the vanishing of the in-plane field. In such a model $B_x = B_z = 0$ at the X-point, making it impossible to satisfy the other requirements there while simultaneously maintaining $E_{\parallel} = 0$. When the model includes a guide field in this work we only consider particle trajectories that do not cross the $z = -\sqrt{\alpha}x$ separatrix.

B. Numerical Results

In order to explore the reversibility of individual trajectories, we introduce test particles into the model's magnetic and electric fields. The field configuration remains fixed as the positions and velocities of the particles are integrated forward in time using the non-relativistic Newton-Lorentz equations: $d\mathbf{x}/dt = \mathbf{v}$ and $d\mathbf{v}/dt = q(\mathbf{E} + \mathbf{v} \times \mathbf{B})$. These equations are reversible and so particles followed forward and backward in time should return to their initial locations. (As in Section II A, the variables are assumed to include a suppressed factor representing the dimensional

information. For instance, $q = \pm 1$ for protons or electrons respectively, although in what follows we choose $q = 1$ for simplicity.)

In practice, however, the accumulation of small integration errors has the potential to alter trajectories. These alterations will be of particular significance when particles pass near locations such as X-points or separatrices where the κ^2 parameter, introduced in²¹ and given by the ratio of the radius of curvature of the magnetic field to the particle Larmor radius, most closely approaches values associated with chaotic motion²². Because X-points and separatrices do not fill the domain, the trajectory of every particle that passes near one effectively threads a needle such that any small change can lead to significant deviations when the orbit is tracked backwards in time. Here the deviations arise from numerical errors in solving the governing equations, but in real plasmas analogous behavior can arise from, for instance, small-amplitude electric field fluctuations. To emphasize the analogy with Landau damping: During reconnection in either an actual plasma or a numerical simulation there will always be random fluctuations that sufficiently perturb particle trajectories and destroy fine-scale phase-space structures. When such fluctuations coincide with regions associated with chaotic particle motions, irreversible particle trajectories result.

We follow particle trajectories via a trapezoidal-leapfrog method with the velocity integration employing the Boris algorithm^{23–25}. The analogy with Landau damping argues that exact numerical convergence is impossible (achieving it would effectively imply infinite phase-space resolution), in that for any timestep there will always exist particles whose trajectories cannot be exactly reversed. In this work we have chosen a timestep, $\Delta t = 10^{-3}$, for which trajectories that do not pass close to the separatrices and X-point are reversible, but emphasize that tests with different values of Δt yield qualitatively similar results. In general, reducing Δt will increase the number of particles and length of time for which trajectories are reversible but will not eliminate irreversibility altogether. Here we show trajectories evolved forward in time for 2.5×10^5 steps and then reversed for an equal period.

Figure 2 shows two particle trajectories in the anti-parallel case of the model described in Section II A. At $t = 0$ both have representative thermal velocities, with the perpendicular velocity augmented with the local $\mathbf{E} \times \mathbf{B}$ drift. The particles have the same guiding centers but different phases (offset by $\pi/2$) so that they initially occupy different locations on the same Larmor orbit centered at $x = 1$, $z = 4.5$. Both particles begin upstream and are tracked forward in time (blue lines) as they pass near the X-line and head downstream until, at $t = 250$, the particles have the locations given by the colored circles (top: $(x, z) \approx (20, -3)$; bottom: $(x, z) \approx (27, 6)$). At the

beginning of their trajectories the particles exhibit the expected helical motions about the field with a pitch given by v_{\parallel}/v_{\perp} . Conservation of the adiabatically invariant magnetic moment implies that v_{\perp} varies in proportion to \sqrt{B} so that the pitch decreases (i.e., the helix winds more tightly) at the mirror points and then increases as the particle moves back towards the origin. Magnetic moment conservation begins to break down near the current layer at $z = 0$ due to the decrease in B . Despite having initial conditions on the same Larmor orbit, the blue trajectories clearly differ near the X-point. Once the particles move away from the current layer they re-magnetize, mirror in the increasing field, and again pass through the region of small field. The overall behavior is quite similar to that seen in particle trajectories taken from full PIC simulations of reconnection^{26,27}.

At $t = 250$ the particle positions are marked by circles and their trajectories are then integrated backwards in time (red lines) by replacing Δt with $-\Delta t$ in the discretization of the Newton-Lorentz equations. (Mathematically, identical results are found by keeping Δt unchanged but mapping $\mathbf{v} \rightarrow -\mathbf{v}$ and either $\mathbf{B} \rightarrow -\mathbf{B}$ or both $q \rightarrow -q$ and $\mathbf{E} \rightarrow -\mathbf{E}$.) While both particles at first closely re-trace their inbound trajectories – the blue lines at first cannot be seen because they coincide with the red ones – each eventually acquires a significant deviation after which the incoming and outgoing trajectories are more or less independent.

Figure 3 shows μ , the first adiabatic invariant, for each particle as a function of time. As in Figure 2, μ during the forward trajectory is shown in blue, while that of the reverse is plotted in red. The large spikes correspond to times when the particles approach the X-point and B approaches zero. The inset in each panel displays the times where the forward and backward values notably begin to deviate and the diamonds correspond to those plotted in Figure 2. In the first case the diamonds are shown slightly after the deviation becomes noticeable at $t = 110$ when the particles are oscillating across the current sheet at $(x, z) \approx (7, -1)$.

Figure 4 shows a similar plot for a configuration that includes a uniform guide field $B_y = 1$ and the associated in-plane electric fields given in equation 5. As in the anti-parallel case, the two particles begin with the same velocities and guiding centers (centered at $x = 1, z = 4.4$) but different gyrophases. The Larmor orbits again exhibit variations in pitch as the particles encounter regions where B changes. Notably, however, the presence of the guide field means that the particles' magnetic moment is mostly conserved, the κ^2 parameter of²¹ remains in the non-chaotic regime, and the particles never fully de-magnetize. As a consequence, passing through the central current sheet does not lead to significant differences in the trajectories as it did in the anti-parallel case. Furthermore, as expected, the reversed-in-time trajectories more closely track the forward-

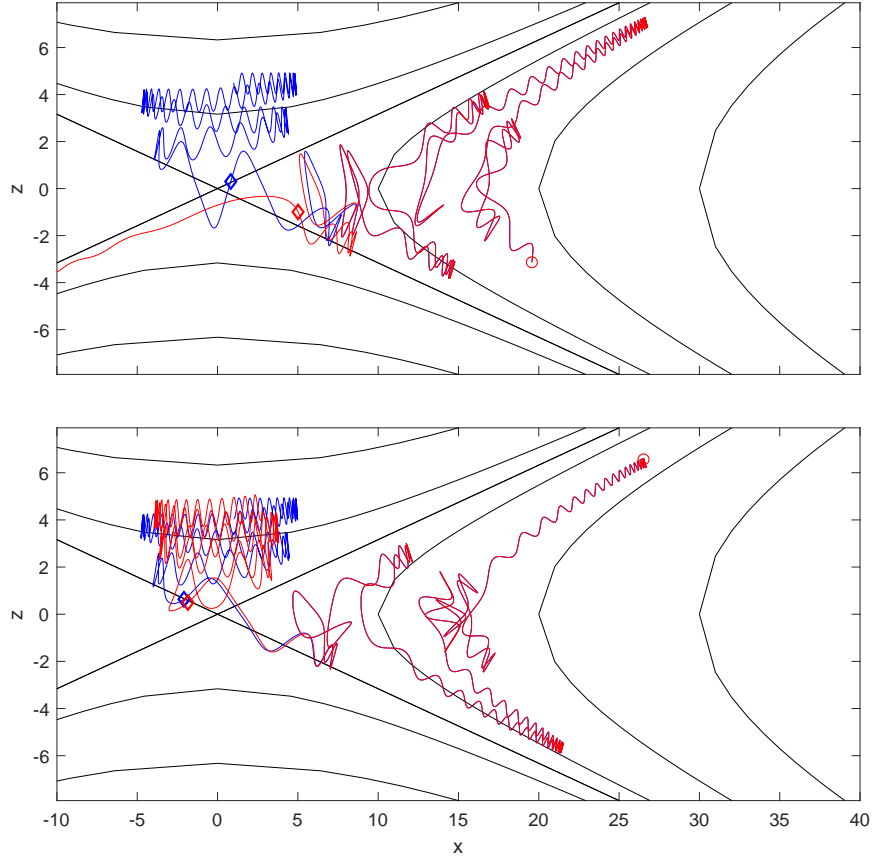


FIG. 2. Magnetic field lines (solid black) and two particle trajectories in the analytic model with $\alpha = 0.1$ and $B_y = E_x = E_z = 0$. Blue lines represent the particle trajectories taken forward in time, red when reversed. Each particle begins on a gyro-orbit centered at $x = 1, z = 4.5$ but separated in phase by $\pi/2$. The locations where the reversals occur are marked by circles. The diamonds indicate the locations discussed in Figure 3. [Associated dataset available at <http://dx.doi.org/10.5281/zenodo.4608531>.]²⁸

in-time motion. In the bottom panel the reversal is nearly exact, with the red reversed trajectory essentially covering the forward blue trajectory.

The results shown in Figures 2 and 4 suggest that the degree of irreversibility is higher in the anti-parallel case. It should be emphasized that the plotted trajectories are meant to be suggestive but not representative. Changes in multiple factors – numerical method, length of integration, timestep, initial position or velocity – will produce different trajectories. A more comprehensive approach comes from examining self-consistent simulations of reconnection.

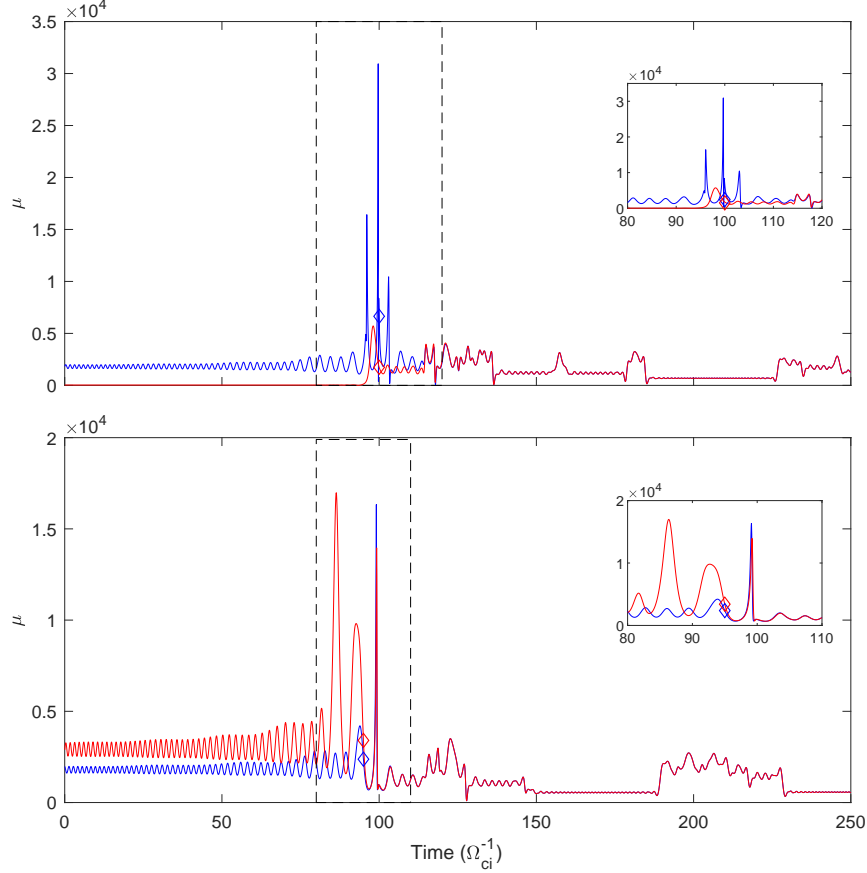


FIG. 3. The first adiabatic invariant μ as a function of time for the particle trajectories shown in Figure 2. The forward trajectory is shown in blue and the reverse in red. The inset of each panel shows a blow-up of the critical region where the forward and backward phases begin to differ significantly. The red and blue diamonds label the points shown marked similarly in Figure 2. [Associated dataset available at <http://dx.doi.org/10.5281/zenodo.4608541>.]²⁹

III. PARTICLE-IN-CELL SIMULATIONS

Particle-in-cell simulations follow the motions of many plasma particles in the self-consistent fields they generate. A key question is whether the results found in Section II for individual trajectories continue to apply. We perform such simulations with the code p3d²⁵. In its normalization a reference magnetic field strength B_0 and density n_0 define the velocity unit $v_{A0} = B_0/\sqrt{4\pi m_i n_0}$ where m_i is the ion mass. Times are normalized to the inverse ion cyclotron frequency $\Omega_{i0}^{-1} = m_i c/eB_0$, lengths to the ion inertial length $d_{i0} = c/\omega_{pi0}$ (where $\omega_{pi0} = \sqrt{4\pi n_0 e^2/m_i}$ is the ion plasma frequency), electric fields to $v_{A0} B_0/c$, and temperatures to $m_i v_{A0}^2$.

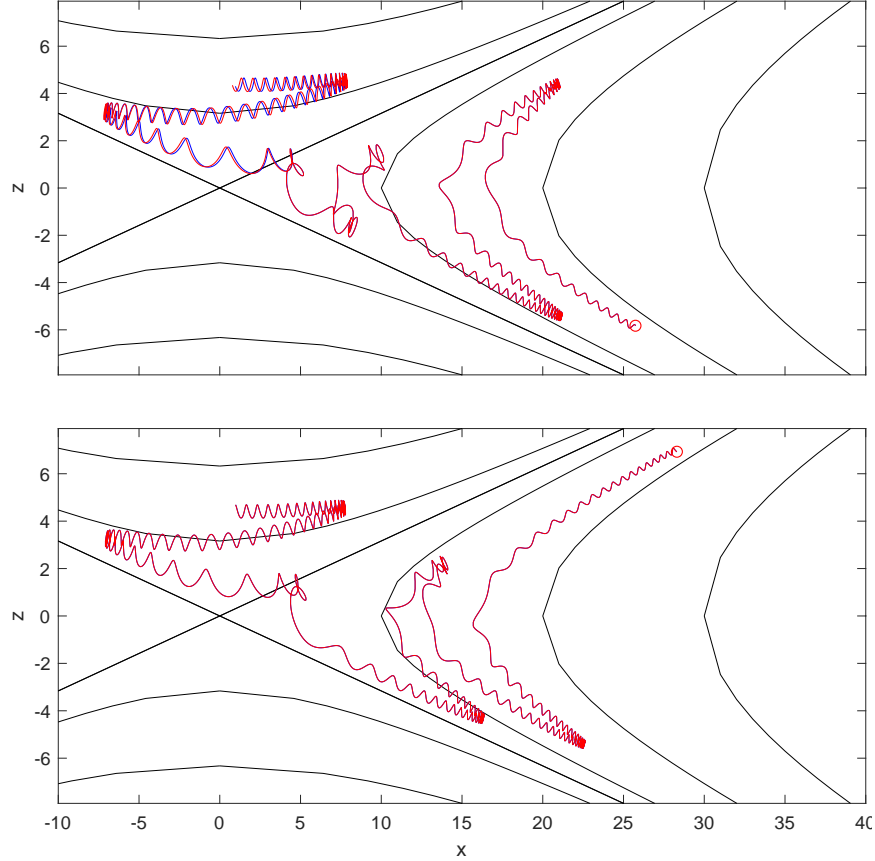


FIG. 4. Magnetic field lines (solid black) and two particle trajectories in the analytic model with $\alpha = 0.1$, $B_y = 1$, and E_x and E_z given by equation 5 in the same format as Figure 2. The particles begin on a gyro-orbit centered at $x = 1, z = 4.4$. In the bottom panel the red reversed trajectory cover the blue forward trajectory. [Associated dataset available at <http://dx.doi.org/10.5281/zenodo.4608551>.]³⁰

The system parameters follow those of the GEM reconnection challenge³¹. The computational domain measures $L_x \times L_z = 25.6 \times 12.8 d_i$. The ion-to-electron mass ratio is taken to be 25, which is sufficient to separate the electron and ion scales (the electron inertial length $d_{e0} = 0.2 d_{i0}$). The electron thermal speed $v_{th,e} \approx 2$ is much less than the normalized speed of light, $c = 20$; the latter further implies that $\omega_{pe}/\Omega_{ce} = 4$. The spatial grid has resolution $\Delta = 0.05$ in normalized units while the Debye length, ≈ 0.04 , is the smallest physical scale. The timestep is $\Delta t = 0.001$. Each grid cell in the initial current sheet contains ≈ 400 macroparticles. The boundaries are periodic in the horizontal direction and conducting perfectly reflecting walls at the top and bottom of the domain. A small perturbation is made to the center of the current sheet at $t = 0$ to begin reconnection.

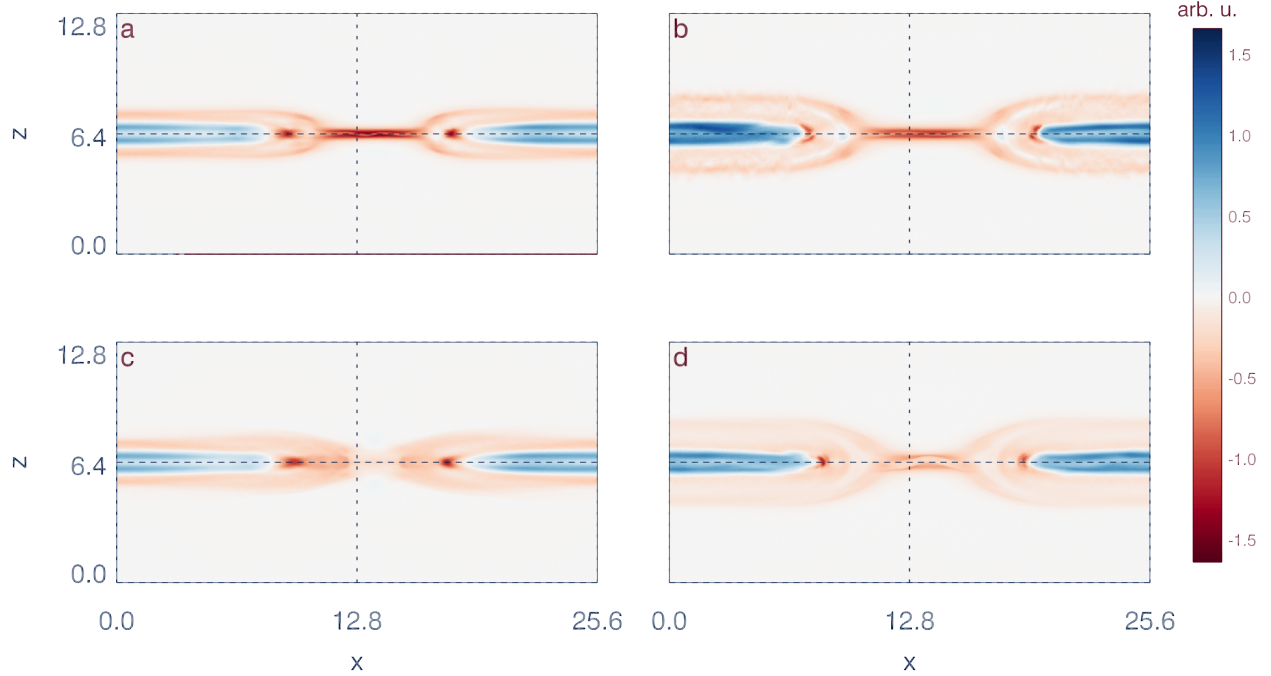


FIG. 5. The out-of-plane electron current density J_{ey} at four times for anti-parallel reconnection. Panel (a) shows field lines and $t = 20\Omega_{ci}^{-1}$. Panel (b) shows $t = 24\Omega_{ci}^{-1}$ when the forward evolution is stopped. Panel (c) shows $t = 20\Omega_{ci}^{-1}$ in the backwards evolution and panel (d) $t = 12\Omega_{ci}^{-1}$. [Associated dataset available at <http://dx.doi.org/10.5281/zenodo.4608554>.]³²

Figure 5 displays the out-of-plane electron current density J_{ey} at four times during the run. Panels a and b display the system at $t = 20\Omega_{ci}^{-1}$ and $t = 24\Omega_{ci}^{-1}$ during the forward time integration. The expected features are present: slowly inflowing plasma, growing islands of reconnected flux and Alfvénic outflow jets (not shown). At $t = 24\Omega_{ci}^{-1}$, panel b, the run is stopped and the backwards integration begun. Depending on the details of the numerical implementation, small errors can be introduced when starting the backwards integration. However, tests with multiple schemes taking more or less care to ensure exact reversibility during the first few time steps yielded essentially indistinguishable results. In the following we simply set $\Delta t \rightarrow -\Delta t$. Panel c shows the system after it has been integrated back to $t = 20\Omega_{ci}^{-1}$ and should be compared to panel a. While some reversal has occurred – in particular, the island widths are similar in panels a and c – the structure of the central current layer is clearly different. Panel d shows the system after it has been evolved further backwards in time to $t = 12\Omega_{ci}^{-1}$. If the system were fully reversible the islands would continue to shrink as flux “unreconnects” and the system would eventually contain a nearly uniform current layer. Instead, reconnection has begun again, as seen in the increase in the island size. The overall

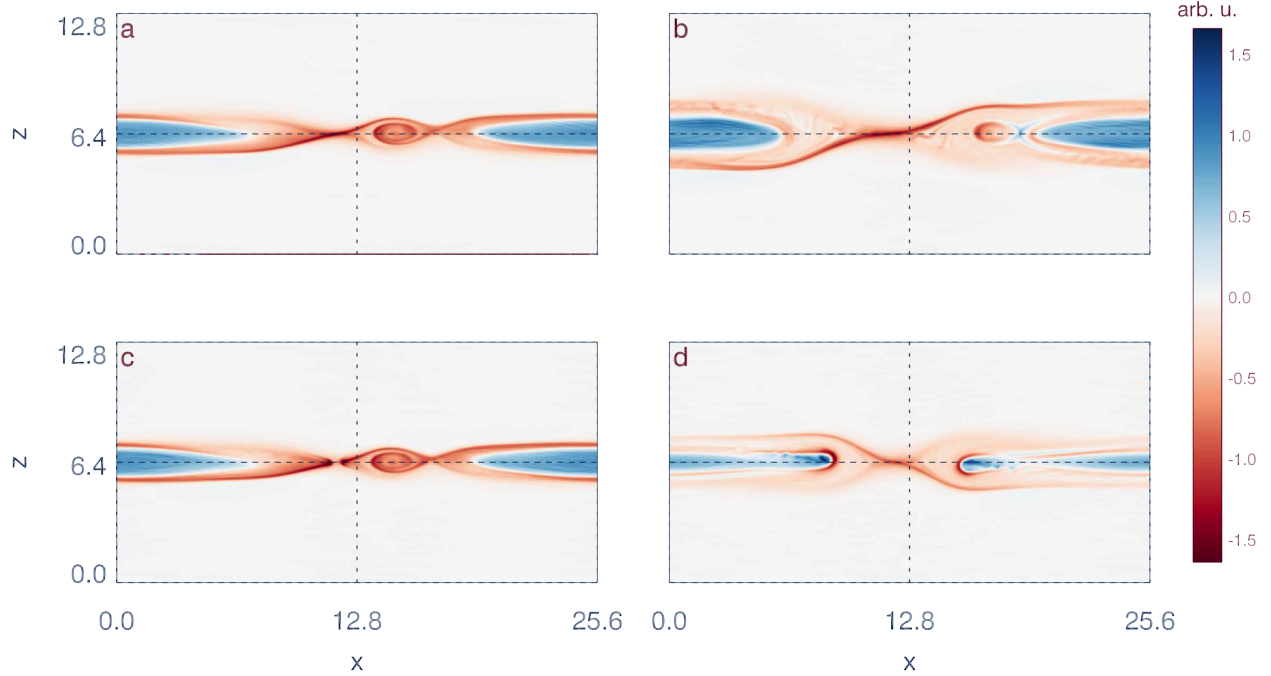


FIG. 6. The out-of-plane electron current density J_y at four times for guide field reconnection with $B_y = 1$ in the same format as Figure 5. [Associated dataset available at <http://dx.doi.org/10.5281/zenodo.4608560>.]³³

morphology closely resembles the state shown in panel b when the time reversal began.

Figure 6 displays the out-of-plane current density at four times for a system that includes an initial uniform guide field, $B_y = 1$, but is otherwise identical to that shown in Figure 5. As before, panels a and b show $t = 20\Omega_{ci}^{-1}$ and $t = 24\Omega_{ci}^{-1}$ from the forward time integration. In this case a plasmoid forms in the slightly narrower current layer near the X-line and moves downstream, nearly fully reconnecting with the flux in the island by the time of panel b. As is typical in guide-field reconnection, one of the separatrices, in this case the one stretching from lower-left to upper-right, is stronger than the other. After the time shown in panel b the backwards integration begins. In panel c (which should be compared to panel a) the plasmoid has emerged from the downstream island and propagated back towards the X-line. The two panels are nearly identical although small differences can be seen, e.g., at $x \approx 11$ and $z \approx 6.4$. However, as the reversed integration continues, reconnection eventually begins again as can be seen in panel d.

A curious feature of the new phase of reconnection is that the strong and weak separatrices switch (compare panels b and d). The morphology of the separatrices before the reversal is a well-understood byproduct of guide-field reconnection and arises from the interaction of E_{\parallel} along the

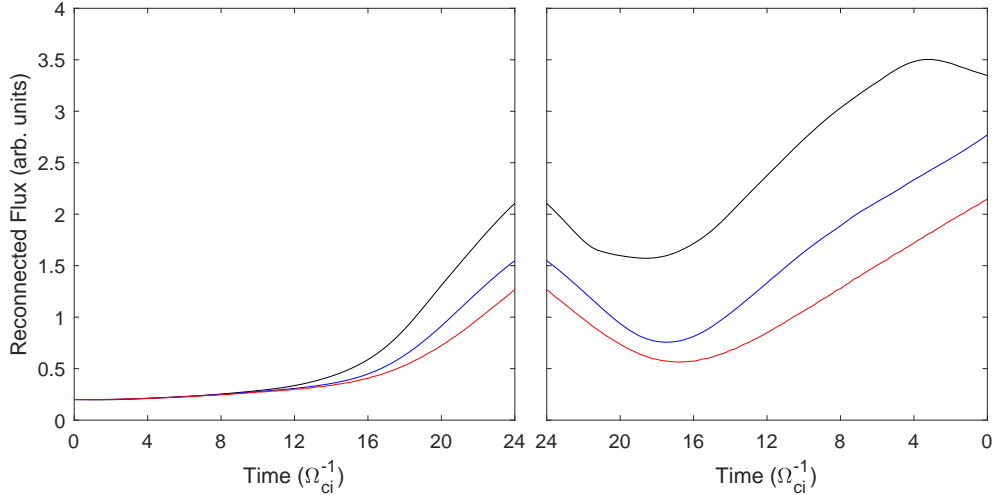


FIG. 7. Reconnected flux versus time for simulations with guide field 0 (black), 1 (blue) and 2 (red). The left panel shows forward integration in time. The right panel, the backward integration. [Associated dataset available at <http://dx.doi.org/10.5281/zenodo.4608562>.]³⁵

separatrices and streaming electrons³⁴. As noted above, reversing the sign of time in the equations governing the system’s evolution (i.e., mapping $t \rightarrow -t$) is mathematically equivalent to keeping t unchanged and instead mapping $\mathbf{B} \rightarrow -\mathbf{B}$ and $\mathbf{v} \rightarrow -\mathbf{v}$. In other words, instead of reversing the flow of time the system can be considered to reverse the direction of the magnetic field and the velocity of every particle in the system instantaneously. Reversing the sign of \mathbf{B} in normal (non-time-reversed) guide-field reconnection reverses which separatrices appear bright and so is consistent with the change in the separatrices shown in panel d.

Figure 7 shows the reconnected flux, as measured by the difference in A_y between the X-point and O-point, versus time for three simulations: The two already discussed and an additional one with $B_y = 2$. The slope of the curve gives the reconnection rate, which is ≈ 0.1 for all three simulations at the time of the reversal. The left panel shows the forward integration, with the vertical offset at $t = 0$ due to the small initial perturbation. Each simulation is run until $t = 24$, the time shown in panel b of Figures 5 and 6. The right panel displays the result of the backward integration. In each case the system retraces its trajectory (“unreconnects”) immediately after the reversal, but eventually stops and then begins to reconnect new flux. As was the case with the test particles discussed in Section II B the systems with guide fields show better reversibility.

Unlike the test particles discussed in Section II B, particles in PIC simulations move on trajectories that evolve based on self-consistently determined electromagnetic fields. In a perfectly

reversible simulation the trajectories from the forward and backward integration would completely overlap but, as might be expected from the irreversibility shown in Figure 7, they do not here. Figure 8 shows the average total displacement between the forward and backward integration of fifty electrons (panel a) and ions (panel b) as a function of time for reconnection with $B_g = 0$ (black curves), $B_g = 1$ (red) and $B_g = 2$ (blue). The particles initially occupied a small region just upstream of the reconnection current sheet. Most passed the separatrices during the simulation and were located in the reconnection outflow when the backwards integration began (this point in time denotes $t = 0$ on the horizontal axis). Because the system is periodic in the horizontal direction and the particles cannot move too far upstream in the y direction due to canonical momentum conservation, the displacement between particles cannot grow without bound. Instead, in all cases the particles initially track their dopplegangers closely before exponentially diverging and then eventually reaching an asymptotic steady-state. As expected, the deviations occur substantially earlier when $B_g = 0$ due to passages through the demagnetized current sheet. As the guide field increases the correlation between the forwards and backwards particles is maintained for longer periods, although eventually divergence occurs for all three cases. While the larger mass of ions (panel b) means larger Larmor radii (and hence less magnetization than electrons), it also increases the gyroperiod; the net result is that the timescale for ion deviation is longer than that for electrons.

IV. DISCUSSION

Previous work³⁷ has demonstrated fully reversible magnetic reconnection in a gyrokinetic simulation of a collisionless plasma. The gyrokinetic equations effectively consider the case of very strong guide field, i.e., a fully magnetized plasma, and hence can be considered a limiting case of the work discussed here. The observed reversibility is consistent with the trend discussed above that increasing the strength of the guide field increases the system's reversibility. The fluid nature of the gyrokinetic model caused the noise levels in the simulations to be quite small (near machine precision), although artificially adding noise led to poorer reversibility. Observations of reconnection have shown it to be accompanied by small-scale electric-field fluctuations that have some similarities to this type of noise^{38,39}. It would be of interest for future work to compare the characteristics (amplitude, spectrum, etc.) of this noise to that in different simulation models in order to assess its possible impact on reversibility.

Irreversibility is closely tied to the question of dissipation of energy. Circumstantial evidence

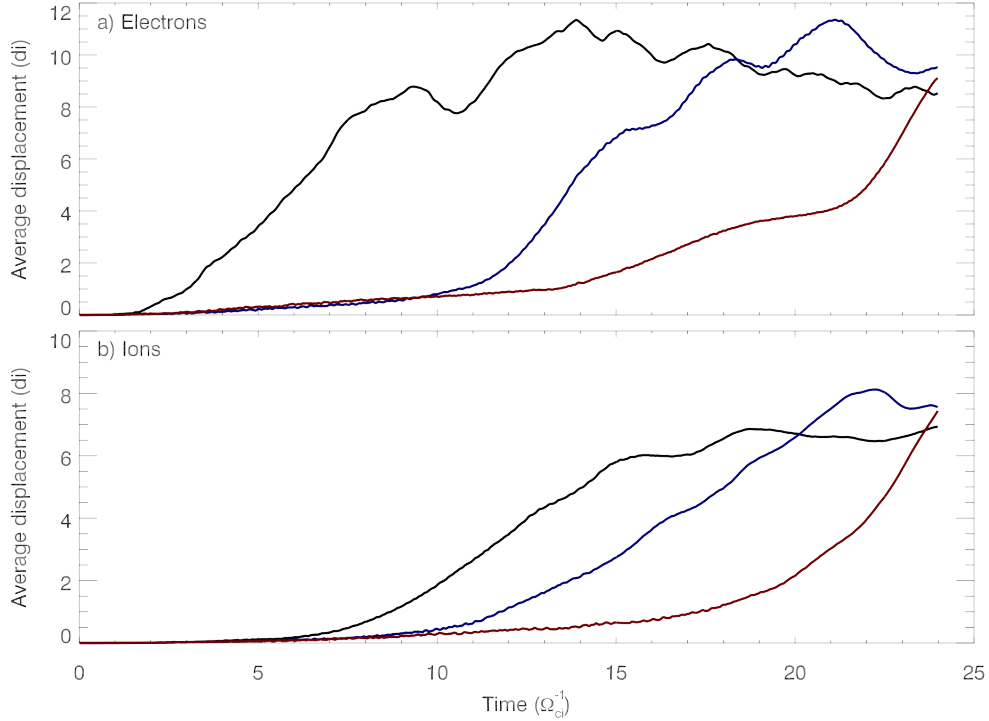


FIG. 8. Average displacement between forward and backward runs as a function of time for electrons (panel a) and ions (panel b). The three curves correspond to runs with guide field 0 (black), 1 (red), and 2 (blue). [Associated dataset available at <http://dx.doi.org/10.5281/zenodo.4608582>.]³⁶

for dissipation during reconnection comes in the form of the observed increase of the downstream plasma temperature^{40,41}. However, definitively proving the existence of irreversible dissipation is not straightforward. A frequently used measure, the identification of regions where $\mathbf{J} \cdot \mathbf{E} > 0$ (where \mathbf{E} is measured in the frame of the electrons⁴²), can be misleading since reversible processes can generate such signals. On the other hand, such signals can be tied to the development of complex structures in phase space. As the complexity increases, weaker and weaker non-ideal processes are sufficient to trigger irreversible heating⁴³.

Determining whether a process is reversible is equivalent to asking whether the entropy remains constant. The generation of entropy in PIC simulations has been a subject of recent study⁴⁴. The kinetic entropy was calculated for collisionless 2.5D anti-parallel reconnection in a closed system. For a simulation with excellent conservation of the total energy, the authors found a monotonic increase in the total entropy of the system, albeit at a low level ($\approx 3\%$ for the entire run). Since the system lacked physical collisions, the entropy increase was attributed to numerical effects. Later work⁴⁵ modelled the entropy increase as an effective numerical collisionality, with the col-

lision frequency dependent on such numerical factors as the resolution, timestep, and number of particles. When considered in the context of this work, these results suggest that reversibility in magnetic reconnection behaves in a manner analogous to Landau damping. In principle every particle in the system follows a trajectory given by the collisionless, reversible equations of motion while the system itself follows a narrow trajectory through a high-dimensional phase space. However, during reconnection the orbits of particles passing near magnetic separatrices and magnetic nulls are sensitive to small perturbations. Deviations from collisionless trajectories (e.g., arising from numerical errors in a simulation or a non-zero effective collisionality in a real system) pushes the plasma off its narrow path in phase space onto an irreversible state. The size of the perturbation needed to effect this change varies, although we have shown that a larger guide field is linked to higher reversibility (and hence smaller entropy increase and energy dissipations).

Several open questions remain. To what degree does reversibility depend on other plasma parameters (e.g., three-dimensionality, β , the magnetization parameter σ that parameterizes relativistic reconnection⁴⁶, or asymmetry across the reconnecting current sheet)? Is it possible for PIC simulations to run in the truly collisionless regime for general reconnection configurations and hence exhibit true reversible behavior? If not, does this have implications for the widely accepted notion that PIC simulations provide a nearly complete picture of magnetic reconnection? And finally, is there a definitive measure of irreversibility and entropy generation that can be evaluated with data obtainable by either spacecraft or laboratory experiments?

ACKNOWLEDGMENTS

The authors acknowledge support from NSF grant No. PHY1805829 and NASA grant 80NSSC19K0396. This research used resources of the National Energy Research Scientific Computing Center, a DOE Office of Science User Facility supported by the Office of Science of the U.S. Department of Energy under Contract No. DE-AC02-05CH11231. Simulation data are available upon request.

REFERENCES

- ¹J. F. Drake, M. Swisdak, H. Che, M. A. Shay, Electron acceleration from contracting magnetic islands during reconnection, *Nature* 443 (2006) 553–556. doi:10.1038/nature05116.

- ²M. Hesse, T. Neukirch, K. Schindler, M. Kuznetsova, S. Zenitani, The diffusion region in collisionless magnetic reconnection, *Space Sci. Rev.* 160 (2011) 3–23. doi:10.1007/s11214-010-9740-1.
- ³P. A. Cassak, Inside the black box: Magnetic reconnection and the Magnetospheric Multiscale Mission, *Space Weather* 14 (2016) 186–197. doi:10.1002/2015SW001313.
- ⁴S. R. Cranmer, A. A. van Ballegoijen, Alfvénic turbulence in the extended solar corona: Kinetic effects and proton heating, *Astrophys. J.* 594 (2003) 573–591. doi:10.1086/376777.
- ⁵N. A. Krall, What do we really know about collisionless shocks?, *Adv. Space Res.* 20 (4–5) (1997) 715–724. doi:10.1016/S0273-1177(97)00461-4.
- ⁶L. Landau, On the vibrations of the electronic plasma, *J. Phys. U.S.S.R.* 10 (1) (1946) 25–34.
- ⁷J. H. Malmberg, C. B. Wharton, Electrostatic damping of electrostatic plasma waves, *Phys. Rev. Lett.* 13 (6) (1964) 184–186. doi:10.1103/PhysRevLett.13.184.
- ⁸A. Y. Wong, R. W. Motley, N. D’Angelo, Landau damping of ion acoustic waves in highly ionized plasmas, *Phys. Rev.* 133 (2A) (1964) A436–A442. doi:10.1103/PhysRev.133.A436.
- ⁹D. D. Ryutov, Landau damping: half a century with the great discovery, *Plasma Phys. Control. Fusion* 41 (3A) (1999) A1–A12. doi:10.1088/0741-3335/41/3a/001.
- ¹⁰E. G. Zweibel, M. Yamada, Magnetic reconnection in astrophysical and laboratory plasmas, *Annu. Rev. Astron. Astrophys.* 47 (2009) 291–332. doi:10.1146/annurev-astro-082708-101726.
- ¹¹J. L. Burch, R. B. Torbert, T. D. Phan, L.-J. Chen, T. E. Moore, R. E. Ergun, J. P. Eastwood, D. J. Gershman, P. A. Cassak, M. R. Argal, S. Wang, M. Hesse, C. J. Pollock, B. L. Giles, R. Nakamura, B. H. Mauk, S. A. Fuselier, C. T. Russell, R. J. Strangeway, J. F. Drake, M. A. Shay, Y. V. Khotyaintsev, P.-A. Lindqvist, G. Marklund, F. D. Wilder, D. T. Young, K. Torkar, J. Goldstein, J. C. Dorelli, L. A. Avanov, M. Oka, D. N. Baker, A. N. Jaynes, K. A. Goodrich, I. J. Cohen, D. L. Turner, J. F. Fennell, J. B. Blake, J. Clemmons, M. Goldman, D. Newman, S. M. Petrinec, K. Trattner, B. Lavraud, P. H. Reiff, W. Baumjohann, W. Magnes, M. Steller, W. Lewis, Y. Saito, V. Coffey, M. Chandler, Electron-scale measurements of magnetic reconnection in space, *Science* 352 (6290). doi:10.1126/science.aaf2939.
- ¹²J. L. Burch, R. E. Ergun, P. Cassak, J. M. Webster, R. B. Torbert, B. L. Giles, J. C. Dorelli, A. C. Rager, K.-J. Hwang, T. D. Phan, K. J. Genestreti, R. C. Allen, L.-J. Chen, S. Wang, D. Gershman, O. L. Contel, C. T. Russell, R. J. Strangeway, F. D. Wilder, D. B. Graham, M. Hesse, J. F. Drake, M. Swisdak, L. M. Price, M. A. Shay, P.-A. Lindqvist, C. J. Pollock, R. E. Denton,

- D. L. Newman, Localized oscillatory energy conversion in magnetopause reconnection, *Geophys. Res. Lett.* 45, (2017) 1237–1245. doi:10.1002/2017GL076809.
- ¹³L. Price, M. Swisdak, J. F. Drake, D. B. Graham, Turbulence and transport during guide field reconnection at the magnetopause, *J. Geophys. Res.* 125 (2020) 1–15. doi:10.1029/2019JA027498.
- ¹⁴W. Daughton, V. Roytershteyn, H. Karimabadi, L. Yin, B. J. Albright, B. Bergen, K. J. Bowers, Role of electron physics in the development of turbulent magnetic reconnection in collisionless plasmas, *Nature Phys.* 7 (2011) 539–542. doi:10.1038/nphys1965.
- ¹⁵M. Hesse, M. Kuznetsova, J. Birn, Particle-in-cell simulations of three-dimensional collisionless magnetic reconnection, *J. Geophys. Res.* 106 (A12) (2001) 29831–29842. doi:10.1029/2001JA000075.
- ¹⁶L. J. D. Craig, G. J. Rickard, Linear models of steady state, incompressible magnetic reconnection, *Astron. Astrophys.* 287 (1994) 261–267.
- ¹⁷D. H. Nickeler, M. Karlický, M. Kraus, Topological structures of velocity and electric field in the vicinity of a cusp-type magnetic null point, *Astrophys. J.* 873 (41). doi:10.3847/1538-4357/ab020b.
- ¹⁸Y.-H. Liu, M. Hesse, F. Guo, W. Daughton, H. Li, P. A. Cassak, M. A. Shay, Why does steady-state magnetic reconnection have a maximum local rate of order 0.1?, *Phys. Rev. Lett.* 118 (2017) 085101. doi:10.1103/PhysRevLett.118.085101.
- ¹⁹M. Swisdak, J. F. Drake, J. McIlhargey, M. A. Shay, The transition from anti-parallel to component magnetic reconnection, *J. Geophys. Res.* 110. doi:10.1029/2004JA010748.
- ²⁰P. L. Pritchett, Geospace environment modeling (GEM) magnetic reconnection challenge: Simulations with a full particle electromagnetic code, *J. Geophys. Res.* 106 (2001) 3783.
- ²¹J. Büchner, L. M. Zelenyi, Regular and chaotic charged particle motion in magnetotaillike field reversals: 1. Basic theory of trapped motion, *J. Geophys. Res.* 94 (A9) (1989) 11821–11842. doi:10.1029/JA094iA09p11821.
- ²²D. F. Escande, R. Paccagnella, S. Cappello, C. Marchetto, F. D’Angelo, Chaos healing by separatrix disappearance and quasisingle helicity states of the reversed field pinch, *Phys. Rev. Lett.* 85 (2000) 3169–3172. doi:10.1103/PhysRevLett.85.3169.
- ²³J. P. Boris, Relativistic plasma simulation-optimization of a hybrid code, in: J. P. Boris, R. A. Shanny (Eds.), *Proceedings of the Fourth Conference on the Numerical Simulation of Plasmas*, Naval Research Laboratory, 1970, pp. 3–67.

- ²⁴C. K. Birdsall, A. B. Langdon, Plasma Physics via Computer Simulation, Institute of Physics Publishing, Philadelphia, 1991, Ch. 15.
- ²⁵A. Zeiler, D. Biskamp, J. F. Drake, B. N. Rogers, M. A. Shay, M. Scholer, Three-dimensional particle simulations of collisionless magnetic reconnection, *J. Geophys. Res.* 107 (A9) (2002) 1230. doi:10.1029/2001JA000287.
- ²⁶L.-J. Chen, N. Bessho, B. Lefebvre, H. Vaith, A. Fazakerley, A. Bhattacharjee, P. A. Puhl-Quinn, A. Runov, Y. Khotyaintsev, A. Vaivads, E. Georgescu, R. Torbert, Evidence of an extended current sheet and its neighboring magnetic island during magnetic reconnection, *J. Geophys. Res.* 113 (2008) A12213. doi:10.1029/2008JA013385.
- ²⁷J. Egedal, J. Ng, A. Le, W. Daughton, B. Wetherton, J. Dorelli, D. J. Gershman, A. Rager, Pressure tensor elements breaking the frozen-in law during reconnection in earth's magnetotail, *Phys. Rev. Lett.* 123. doi:10.1103/PhysRevLett.123.225101.
- ²⁸M. Xuan, M. Swisdak, J. F. Drake, Fig 2, Dataset (2021). doi:10.5281/zenodo.4608531.
- ²⁹M. Xuan, M. Swisdak, J. F. Drake, Fig 3, Dataset (2021). doi:10.5281/zenodo.4608541.
- ³⁰M. Xuan, M. Swisdak, J. F. Drake, Fig 4, Dataset (2021). doi:10.5281/zenodo.4608551.
- ³¹J. Birn, J. F. Drake, M. A. Shay, B. N. Rogers, R. E. Denton, M. Hesse, M. Kuznetsova, Z. W. Ma, A. Bhattacharjee, A. Otto, P. L. Pritchett, Geospace Environmental Modeling (GEM) magnetic reconnection challenge, *J. Geophys. Res.* 106 (A3) (2001) 3715–3719. doi:10.1029/1999JA900449.
- ³²M. Xuan, M. Swisdak, J. F. Drake, Fig 5, Dataset (2021). doi:10.5281/zenodo.4608554.
- ³³M. Xuan, M. Swisdak, J. F. Drake, Fig 6, Dataset (2021). doi:10.5281/zenodo.4608560.
- ³⁴P. L. Pritchett, F. V. Coroniti, Three-dimensional collisionless magnetic reconnection in the presence of a guide field, *J. Geophys. Res.* 109 (A1). doi:10.1029/2003JA009999.
- ³⁵M. Xuan, M. Swisdak, J. F. Drake, Fig 7, Dataset (2021). doi:10.5281/zenodo.4608562.
- ³⁶M. Xuan, M. Swisdak, J. F. Drake, Fig 8, Dataset (2021). doi:10.5281/zenodo.4608582.
- ³⁷A. Ishizawa, T.-H. Watanabe, Reversible collisionless magnetic reconnection, *Phys. Plasmas* 20. doi:10.1063/1.4826201.
- ³⁸R. E. Ergun, K. A. Goodrich, F. D. Wilder, J. C. Holmes, J. E. Stawarz, S. Eriksson, A. P. Sturmer, D. M. Malaspina, M. E. Usanova, R. B. Torbert, P.-A. Lindqvist, Y. Khotyaintsev, J. L. Burch, R. J. Strangeway, C. T. Russell, C. J. Pollock, B. L. Giles, M. Hesse, L. J. Chen, G. Lapenta, M. V. Goldman, D. L. Newman, S. J. Schwartz, J. P. Eastwood, T. D. Phan, F. S. Mozer, J. Drake, M. A. Shay, P. A. Cassak, R. Nakamura, G. Marklund, Magnetospheric multiscale satellites

- observations of parallel electric fields associated with magnetic reconnection, *Phys. Rev. Lett.* 116. doi:10.1103/PhysRevLett.116.235102.
- ³⁹R. E. Ergun, L. J. Chen, F. D. Wilder, N. Ahmadi, S. Eriksson, M. E. Usanova, K. A. Goodrich, J. C. Holmes, A. P. Sturmer, D. M. Malaspina, D. L. Newman, R. B. Torbert, M. Argall, P.-A. Lindqvist, J. L. Burch, J. M. Webster, J. Drake, L. M. Price, P. A. Cassak, M. Swisdak, M. A. Shay, D. B. Graham, R. J. Strangeway, C. T. Russell, B. L. Giles, J. C. Dorelli, D. Gershman, L. Avanov, M. Hesse, B. Lavraud, O. L. Contel, A. Retino, T. D. Phan, M. Øieroset, M. V. Goldman, J. E. Stawarz, S. J. Schwartz, J. P. Eastwood, K.-J. Hwang, R. Nakamura, S. Wang, Drift waves, intense parallel electric fields, and turbulence associated with asymmetric magnetic reconnection at the magnetopause, *Geophys. Res. Lett.* 44. doi:10.1002/2016GL072493.
- ⁴⁰T. D. Phan, M. A. Shay, J. T. Gosling, M. Fujimoto, J. F. Drake, G. Paschmann, M. Øieroset, J. P. Eastwood, V. Angelopoulos, Electron bulk heating in magnetic reconnection at earth's magnetopause: Dependence on the inflow Alfvén speed and magnetic shear, *Geophys. Res. Lett.* 40 (17) (2013) 4475–4480. doi:10.1002/grl.50917.
- ⁴¹C. C. Haggerty, M. A. Shay, J. F. Drake, T. D. Phan, C. T. McHugh, The competition of electron and ion heating during magnetic reconnection, *Geophys. Res. Lett.* 42 (2015) 9657–9665. doi:10.1002/2015GL065961.
- ⁴²S. Zenitani, M. Hesse, A. Klimas, M. Kuznetsova, New measure of the dissipation region in collisionless magnetic reconnection, *Phys. Rev. Lett.* 106 (19). doi:10.1103/PhysRevLett.106.195003.
- ⁴³M. Swisdak, J. F. Drake, L. Price, J. L. Burch, P. A. Cassak, T.-D. Phan, Localized energy conversion in the diffusion region of asymmetric magnetic reconnection, *Geophys. Res. Lett.* 45 (2018) 5260–5267. doi:10.1029/2017GL076862.
- ⁴⁴H. Liang, P. A. Cassak, S. Servidio, M. A. Shay, J. F. Drake, M. Swisdak, M. R. Argall, J. C. Dorelli, E. E. Scime, W. H. Matthaeus, V. Roytershteyn, G. L. Delzanno, Decomposition of plasma kinetic entropy into position and velocity space and the use of kinetic entropy in particle-in-cell simulations, *Phys. Plasmas* 26. doi:10.1063/1.5098888.
- ⁴⁵H. Liang, P. A. Cassak, M. Swisdak, S. Servidio, Estimating effective collision frequency and kinetic uncertainty in particle-in-cell simulations, *J. Phys. Conf. Ser.* 1620. doi:10.1088/1742-6596/1620/1/012009.
- ⁴⁶F. Guo, H. Li, W. Daughton, Y.-H. Liu, Hard power laws in the energetic particle spectra resulting from relativistic magnetic reconnection, *Phys. Rev. Lett.* 113. doi:10.1103/PhysRevLett.

113.155005.